Pharmacological and in vitro study of probucol-lithocholic acid micro-nanocapsules to prevent the hearing impairment induced by oxidative stress. A preliminary study

Susbin Raj Wagle
Curtin University
Corina Mihaela Ionescu
Curtin University
, Bozica Kovacevic
Curtin University
Melissa Jones
Curtin University
Thomas Foster
Curtin University
Patrick Lim
Curtin University
Michael Lewkowicz
Curtin University
Elaine YM Wong
Hearing Therapeutics Department, Ear Science Institute Australia, Queen Elizabeth II Medical Centre, Nedlands 6009, Perth, Western Australia
Maja DJanic
University of Novi Sad
Momir Mikov
University of Novi Sad
Armin Mooranian
Curtin University
Hani Al-Salami (hani.al-salami@curtin.edu.au)
Curtin University

Article

Keywords: Sensorineural hearing loss, oxidative stress, probucol, lithocholic acid, encapsulation

Posted Date: May 26th, 2022

DOI: https://doi.org/10.21203/rs.3.rs-1644125/v1

Abstract

Pathophysiology of sensorineural hearing loss (SHL) has been associated with oxidative stress. Earlier studies have shown that Probucol (PB) microcapsules can prevent oxidation and inflammation induced by reactive oxygen species in pancreatic β-cells. Therefore, we hypothesised PB containing capsules might prevent the development of hearing impairment caused by oxidative stress. However, PB has many limitations to achieving maximum therapeutic dose, which can be achieved by optimised formulation. Thus, this study aims to design a novel, stable formulation of PB using polymers with and without lithocholic acid (LCA) as an excipient, and examine the efficiency of these formulations on the House Ear Institute-Organ of Corti 1 (HEI-OC1) cell line. The PB was encapsulated using the spray-drying technique and tested for particle characterization and *in vitro* effectiveness. This study demonstrates that all formulations yielded uniform, circular microcapsules with consistent surface topography. The addition of LCA did not affect drug content, but its effect was noticeable on surface chemistry and electrokinetic stability. The addition of LCA favoured controlled drug release kinetics. Cell viability, bioenergetics parameters and inflammatory profile improved when cells were exposed to PB-LCA microcapsules ($p < 0.05$). Therefore, the PB-LCA microcapsule can potentially prevent SHL induced by oxidative stress.

Introduction

Sensorineural hearing loss (SHL) is a subset of clinical hearing loss, associated with loss of hearing sensitivity due to cell death and/or peripheral tissue damage in the cochlea. The underlying causes of SHL are multifactorial; presbycusis, certain drugs, overexposure to sound, immune-induced inflammation, infection or disorders such as diabetes and high blood pressure are all common causes. The pathophysiology of SHL is not fully understood; however, numerous studies have reported that the development of chronic oxidative stress may be associated with SHL pathogenesis regardless of causes 1–3.

Lower intrinsic anti-oxidant defence mechanism and high metabolic demand of hair cells means the cochlea is tremendously vulnerable to oxidative stress 4. Therefore, increased reactive oxygen species (ROS) production in the cochlea can cause cellular dysfunction, impaired blood flow and degeneration of the stria vascularis supporting structures and nerve cells 5,6. Moreover, different histological studies show oxidative stress in mice leads to loss of inner and outer hair cells 7,8, atrophy of spiral ganglion cells, thinning of the stria vascularis and atrophy of the spiral ligament 9,10.

Considering the importance of oxidative stress in the pathophysiology of SHL, different anti-oxidants have been previously studied to prevent oxidative induced SHL 11,12. Accordingly, the question of whether anti-oxidants could have a favourable outcome in decreasing SHL risk has been intensively studied, but the results remain indecisive and controversial12-14. In summary, the fact cannot be denied that there is a genuine need for a novel, and effective, medication superior to current treatments, potentially, relying on anti-oxidants to play a key role in preventing SHL 9,13,15.

Probucol (PB) is a potent anti-hyperlipidemic drug with anti-oxidant and anti-inflammatory properties. The active compound in PB is a bisphenol with butylated hydroxytoluene rings linked together with sulphur carbon bonds. PB shows anti-oxidant activities by both breaking the free radical chain reaction by hydrogen atom transfer, or electron transfer, and also by inducing the endogenous anti-oxidant system 16,17. Moreover, it also directly protects DNA strands from ROS. PB has proven its effectiveness in many organs and tissues as a potent antioxidant 18,19. As a step toward the development of a drug against diabetes mellitus, PB has also shown its potential by protecting pancreatic β-cells from inflammation and oxidation levels 20. However, PB is highly lipophilic, has poor bioavailability, lower absorption kinetics and is prone to inter-and intra-individual variations in dose recipient patients 21.

One possible approach to overcome the obstacles faced by PB is to develop, and optimise, novel and stable formulations that protect the drug from unwanted degradation, increase drug solubility, and ultimately release the drug at the target site in a controlled manner without having toxic off target effects. A step in achieving this would be by implementing encapsulation technology. Spray drying is one of the physical encapsulation techniques that converts a liquid phase into a dry, solid, powder and produces nano-sized particles that can easily pass from the tissue to the target site, increasing bioavailability and therapeutic efficacy. Therefore, many studies have clarified the significance of nanoparticles as a promising drug-delivering method to the inner ear 22.

Drugs encapsulated in nanoparticles and delivered directly into the middle ear appear advantageous. Drugs can enter the inner ear, diffusing into the perilymph fluid while offering controlled and sustained drug release kinetics. However, *in vivo* studies have shown that sustained drug release by intratympanic injection has more consistent clinical outcomes, showing more drug permeation deep in the temporal bone 23,24, but many studies fail to produce capsules that support controlled drug release 24–26.

Over the last ten years, bile acids (BA) s have become an attractive excipient in drug delivery research. Due to their unique amphoteric properties BAs can support drug absorption and permeation via biological membranes, and act as a drug carriers and stabiliser by forming micelles, bilosomes, and chemical conjugates with drug compounds 20,27–31. These properties makes BAs powerful physiological surfactants and facilitates the encapsulation of both non-polar and polar compounds.

Overall, more than one hundred different kinds of bile acids are present endogenously inside the human body. Different studies have previously successfully used some common bile acids as excipients, developing novel and powerful PB based capsules that showed effectiveness in preventing diabetes mellitus 20,29,32,33. Incorporation of lithocholic acid (LCA) with PB in microcapsule formulations showed positive cellular effects, with reduced oxidation and inflammation on diabetic pancreatic β-cells, and supported controlled and targeted drug release without compromising PB's physical and chemical characteristics 34,35.

Developing nanocapsules, which support the controlled drug release, could be one novel approach for treating hearing impairment. Many factors play a role in how much drug is available in the inner ear; the

round window membrane permeability, drug particle size, drug solubility, drug stability, biocompatibility, electric charges and rheological parameters 36. Therefore, designing a stable formulation is challenging for delivering a drug to treat SHL. Hence, the study's objective was to form advanced nanocapsules of PB with LCA, which would support the sustained and controlled release of PB, assess the *in vitro* impact of PB-LCA capsule, and make a platform for the *in vivo* study using intratympanic drug delivery method.

Results And Discussion

Characterisation of micro-nanocapsules

Physical characterisation of micro-nanocapsules based on morphology and surface elemental analysis

Figure 1 shows that F1, F2 and F3 show the images obtained by SEM. Spherical shape and uniformity in size morphology of the aggregates was observed. The average diameter of nano-microcapsule was 1.313 ± 0.622 µm, 1.466 ± 0.71 µm and 1.02 ± 0.39 µm for F1, F2 and F3 respectively (Table 1). The addition of LCA in formulation F3 statistically significantly decreased the size compared to F1 ($p < 0.05$). The decrease in F3 size, brought by LCA, is attributed to nano-microcapsules having a high surface area to volume ratio, cohesiveness and curvature, which means a greater amount of drug can come into contact with the nano-microcapsules core. Thus, this may impact the efficacy of the drug in *in vivo* studies and result in increased dissolution rates of the drug 37. Generally, spray dry technology produces capsules in agglomerates as seen in **Fig. 1 (i-vi)**. It could be more advantageous in influencing prolonged drug retention and higher drug concentration *in vivo* compared to conventional particle morphology 20,37,38.

Likewise, Table 1 shows the surface elemental analysis of microcapsules analysed by EDS. The EDS spectra of all the micro-nanocapsules showed the presence of different atoms; carbon (C), oxygen (O), and sodium (Na). In our previous studies, PB microcapsules presented with the sulphur (S) atom on the surface of the capsule, demonstrating the confirmation of PB on the surface of the capsule 35,39. However, the present study does not show PB presence on the surface of microcapsules. PB may likely be present inside the capsule core, which indicates a better, robust, and optimised formulation. The dominant atom present on EDS spectra composed largely composed of sodium alginate dominant by C, O and Na atoms 40.

Table 1
Surface elemental analysis of different formulations. The size of capsules is determined by image J analysis software. Level of significance, $p < 0.05$.

Formulations	*Size of capsules (µm)*	*Major surface elemental distribution*
F1	1.31 ± 0.62	N, C, O, and Na
F2	1.46 ± 0.71*	N, C, O, and Na
F3	1.02 ± 0.39*	N, C, O, and Na
Statistically significant difference (p > 0.05)	F2 vs F3	

Rheological, electrokinetic stability, surface tension, thermal and chemical analysis

Rheological parameters such as viscosity, shear rate, torque and shear stress are presented in **Fig. 2 (A-C)**. The parameters were recorded at various set speeds (20-1000 rpm). The rheological patterns showed a parallel reduction in their apparent viscosity, increase in torque and share stress under increasing stress rate. In summary, this indicated that all the formulations acted as non-Newtonian, thixotropic fluids 41,42. All the formulations form rapid circular motions away from the origin of centripetal forces while the set speed is increased, suggesting the non-Weissenberg fashion particle formulations 41,43. The LCA incorporation did not change the fluidic mechanics of formulation F3. The fluid behaviour is important to understanding capsules stability profile, fabrication, and drug release kinetics, which is parallel with previous studies 35,44.

The electrokinetic stability of all the formulations is presented in Table 2. Remarkably, the addition of LCA in the F3 formulation significantly improved the stability of the formulation. The magnitude of the negative charge of microcapsules has previously been reported to be proportional to with stability and dispersion of the solution, which in turn, results in particle flocculation and agglomeration45,46. Likewise, Table 2 further highlights the surface chemistry of the particles. By incorporating LCA there is a noteworthy decrease in surface chemistry of the liquid's formulation which means LCA supports easier spreading over the surface, making a thin and soft layer of liquid suspension that helps the smooth flow of liquid from the nozzle of spray dry and more importantly this behaviour increase the drug distribution and absorption 47.

The excipient-drug thermal melting temperature compatibilities were analysed using the DSC. The thermal peak of PB powder 126.8 ± 1.5°C, LCA 187.2 ± 2°C and SA 194 ± 3°C were reported, which correspond appropriately with each respective melting point, as per our previous study 35. Likewise,

poloxamer, PVA, PAA and silk fibre protein melting points were noted at 55 ± 3°C, 191 ± 1°C, 120 ± 2°C and 151.8 ± 2°C respectively. Gelatin shows a single, wide, thermal peak at 98.0°C ± 5. During the pre-micro-nanocapsule processes (mixture of a free compound), three major characteristic peaks were noted; 43.5 ± 1.55°C, PB peak at 126.67 ± 0.75°C and next, possibly SA, peak at 179.9 ± 3.54°C. F1 presented three major peaks at 43.1 ± 0.6°C, 93.6 ± 6.3°C and 195.15 ± 1.05°C corresponding primarily to poloxamer, gelatin and perhaps the combined peak of SA-PVA. Likewise, F2 micro-nanocapsules also presented three major thermic peaks at 43.5 ± 0.5°C, 126.8 ± 0.4°C and 182.85 ± 1.85°C. Similar to F2, F3 has three major thermic peaks at 44.1 ± 0.9°C, PB peak at 126.7 ± 0.3°C and probably SA-LCA peak at 181.15 ± 2.15°C (Table 2). It is interesting to note that in the pre and post-micro-nano encapsulation process, SA and LCA peaks merge, resulting in a marginal exothermic shift in thermal peak towards the left when compared to their corresponding powder to form one major peak and are involved in an ionic-crosslinking reaction. Perhaps due to alternation in the plasticisation, crystallinity and polymorphism, but interestingly this unification does not alter the thermal characteristic of PB, which closely aligns with the authors' previous studies35,43. The crosslinking between SA and LCA makes capsules more stable, with the ability to resist unwanted mechanical pressure, and stress and may increase membrane stability 48. Not only SA and LCA but also the other added polymers do not affect the thermal compatibilities of PB and possibly, they may interact with each other to form better cross-links, which is also buoyed by FT-IR results (Table 2).

The chemical bond stability and alternation of PB with the addition of SA, LCA and other polymers were established by identifying the functional groups present within a molecule or between molecules using the FT-IR method 49. Only the major and characteristic peaks specific to a particular compound were noted. FT-IR PB spectra showed primarily three specific peaks at 2957.94 cm^{-1}, 1422.06 cm^{-1}, and 1309 cm^{-1} which are parallel to O-H, C-H and S = O functional groups respectively. Likewise, SA displays four peaks; O-H intense stretching peak at 3235.5 cm^{-1}, C-H intense stretching peak at 1406.9 cm^{-1} and 1025.88 cm^{-1} and C = C intense stretching peak at 1599.2 cm^{-1}. Moreover, LCA showed four major characteristic spectra at 3285.3 cm^{-1} 2924.84 cm^{-1} 1700.93 cm^{-1} and 1040 cm^{-1}, similar to our previous work 35. The structural determination of poloxamer, gelatine, PVA, PAA and silk fibre protein display stretching intense peaks similar to other studies 50–56. Parallel with the DSC results, pre-micro-nanocapsules display the distinctive peaks of PB at 1422 cm^{-1} and 1309 cm^{-1} suggesting excipient compatibility and stability of PB even after the addition of LCA with no interference. The SA and LCA spectra combined to form one common peak at 1031 cm^{-1} which supports our DSC result. As shown in Table 2, F1 micro-nanocapsule mostly showed the characteristic peaks of SA. F2 micro-nanocapsules show interference-free peaks at 1309 cm^{-1}, representing PB. Similar interference free peaks at 1308 cm^{-1} of PB were also noticed in F3 micro-nanocapsules suggesting PB chemical stability in these formulations. Parallel to DSC analysis, SA and LCA, the characteristic peak of LCA and SA combine and give one common peak during encapsulation process at 1031 cm^{-1} in F2 and 1032 cm^{-1} in F3 cm^{-1}. However, this interaction and addition of other polymers does not affect chemical modification of PB. Thus, from DSC and FT-IR results, it is clear that encapsulation of PB with SA, LCA and other polymers does not significantly negotiate the structural, thermal and chemical integrity of PB.

Drug content and release study

As shown in Table 2, even though the addition of LCA in F3 increased the PB content it is not statistically significant compared to F2 *(p* > 0.05), which shows that LCA addition does not change the concentration of PB, supporting the authors' previous studies 48,57. However, the impact of LCA addition is seen in the PB release profile presented in **Fig. 2D**. The drug content and release study support our hypothesis that PB is present on the inner core of the capsules rather than on the capsule's shell. This also means, early drug release from both the capsules is low due to the PB present inside the core of the capsules rather on the surface as shown in the EDS result (Table 1).

Release studies show that from 30 minutes to 2 hours, PB release from the F2 is rapid and higher compared to F3, but statistically not significant. However, after 2 hours a PB rapid and "burst release" from F3 was observed to be statistically significantly greater compared to F2 ($p < 0.05$). The result proved that the inclusion of LCA established an improvement in drug release, which means this drug release study is formulation dependent20,35,39. From the physicochemical compatibility study **(**Table 2**)**, it is clear that SA and LCA cross-link with each, strengthen the wall of the encapsulation matrix, and prevent the rapid degradation of PB. These features support a more controlled release of the drug in the early hours. After a certain time, alginic acid forms a soluble viscid layer due to quick solubilisation and dissolution that break the cross-link bond with LCA. This mechanism causes a rapid release of the drug, which was intact inside the core of the capsules. After 3 hours, the drug release from both formulations reached a stable profile with maximum release from the F2 formulation at 62 ± 4% and from F3 at 79 ± 2% ($p < 0.05$) (Fig. 2D). Both formulations provide sustained drug release.

Controlled and sustained drug release formulations are important to decrease the concentration of drugs needed to show the maximum positive effect of the drug in patients with cochlear dysfunction. Studies show that controlled, sustained drug release into the inner ear determines the ultimate outcome of the drug and prevents the unwanted drain of the drug into the Eustachian tube 24. Together with controlled drug release, burst release has been utilised to deliver drugs at high release concentrations as a targeted delivery strategy 58. However, researchers chase to avoid initial burst release, with potential reasons being, that high drug release at the starting phase could cause drug toxicity and may also be metabolised and excreted without being utilised effectively 59,60. In our previous study, drug release from SA microcapsules showed early burst and uni-phasic PB release even after the addition of taurocholic acid (another bile acid), probably due to the presence of PB 39. However, the addition of both natural and synthetic polymers and LCA and improved methodology could give better and improved PB release patterns in this study. The LCA addition showed a decrease in the size of capsules and surface chemistry and better electrokinetic stability; this could be another reason why the PB-LCA microcapsule showed controlled release kinetics.

In the last few years, silica-based nanoparticles and viral vector systems have been highly utilized to deliver drugs to the inner ear. Every delivery system has pros and cons, for example, viral vector is still considered harmful to the delivery drug and silica-based nanoparticles have limited controlled drug

release, limiting drug clearance by drainage from the Eustachian tube or elimination out of the blood lybrithium barriers 25. In addition, silica-based nanoparticles may cause prolonged diffusion across the round window membrane cavity 61,62. Therefore, our robust formulation preserved initial burst release and supported controlled and sustained drug release and control degradation kinetics, which might be the best approach for targeted drug transfer to the round window membrane.

Table 2
Zeta potential, surface tension, drug content DSC and FTIR analysis. Data are presented as mean ± standard deviation, n = 3. Level of significance, $p < 0.05$.

Formulations	*Zeta potential (mV)*	*Surface tension (mN/m)*	*Drug Content (%)*	*DSC (°C) major thermal peaks*	*FTIR* (cm^{-1}) major characteristic spectral
F1	-12.57 ± 4.31	61.50 ± 2.06 *		43.1 ± 0.6, 93.6 ± 6.3 and 195.15 ± 1.05	3346, 2889, 1733, 1606, 1412 and 1031
F2	-13.02 ± 4.63	66.33 ± 2.92 *	5.66 ± 0.92	43.2 ± 1.3, 126.07 ± 1.17 and 179 ± 3.23	3222, 2952, 1870, 1605, 1415, 1309 and 1031
F3	-23.36 ± 7.69	51.33 ± 3.19 *	6.29 ± 1.29	44.1 ± 2.5, 26.66 ± 0.72 and 180 ± 0.92	3290, 2954, 2860, 1701, 1416, 1308 and 1032
Statistically significant difference ($p > 0.05$)	F1 vs F3 F2 vs F3	F1 vs F2 F1 vs F3 F2 vs F3			

In vitro **efficacy of characterised micro-nanocapsules**

Effect on cell viability

Figure 3 (A and B) shows the effect of F1, F2 and F3 micro-nanocapsules on the cell viability of HEI-OC1 cells. The data was normalised where 100% is the viability of cells, which is, consider as control (C1). The percentage of cell viability significantly improved when cells were exposed to F2 and F3 ($p < 0.05$). The cellular viability of C2 and F1 were below 50%, whereas cellular viability significantly increased, to ~ 70% when cells were treated with F2 and F3 micro-nanocapsules ($p < 0.05$). The highest increase was noticed when cells were treated with F3 ($p < 0.05$) (Fig. 3A). Cellular staining of live/dead cells was presented in

Fig. 3B to complement the MTT results. The number of dead cells significantly increased in the untreated group (C2) and F1, while fewer dead cells were observed when cells were treated with F2 and F3 micro-nanocapsules. This result suggest the PB acts as an anti-oxidant and protects HEI-OC1 from the oxidative damage usually caused by AAPH, resulting in the normalisation of free radicals. The protective effect brought by PB is significantly enhanced in the presence of LCA, which is consistent with our previous works showing a protective effect of PB-bile acids on pancreatic β-cells from oxidation and inflammation 35,63. The positive effects of F3 micro-nanocapsules (Fig. 4) may be due to the increased PB release once LCA is added (Fig. 2D), or due to the anti-apoptotic or anti-inflammatory effects of LCA 64,65. AAPH is an azo compound, generating peroxyl radicals forming in the reaction with oxygen peroxyl radicals and often causes lipid peroxidation and cellular oxidative damage without generating hydrogen H_2O_2 as an intermediate 66. Thus, PB-LCA micro-nanocapsules are shown to reverse this mechanism and protect the cells, which positively influences other biological data (Fig. 4).

Effect on bioenergetics assay

Figure 4 (A-C) shows the cellular respiration and mitochondrial activity of HEI-OC1 cells when measured after cells were exposed to AAPH and treated with and without nano-microcapsules. The results are in line with the cell viability assays, which shows statistically significant improvement in bioenergetics parameters when cells are treated with F2 and F3 micro-nanocapsules ($p > 0.05$), which is similar to our previous studies 35,48. The addition of F3 nano-microcapsule to the cells treated with APPH significantly increased the OCR from − 53 ± 1.02 to 187 ± 11.76 pmol O_2/min, suggesting an increase in mitochondrial respiration **(Fig. 4A)**. Moreover, it signifies a higher OCR, likely linked with high ATP (adenosine triphosphate) turnover and electron transfer with a proportional increase in oxidative phosphorylation due to low mitochondrial damage 67. Increased ECAR from 35.50 ± 0.55 to 99.40 ± 6.8 mpH/min and PPR from 63.75 ± 1.75 to 174.45 ± 12.78 pmol/min when treated with F3 micro-nanocapsule **(Fig. 4B-C)**, suggests more proton transport, supporting the production of cellular energy via the glycolysis pathway and complements OCR results **(Fig. 4A)**. Through the glycolysis pathway, pyruvate in the presence of oxygen is oxidised to NADH, forming a proton gradient from ATP-ADP, changing the ATP: ADP ratio and increasing the cellular ATP production. It signifies the synthesis of oxygen molecules in the mitochondrial electron transport chain has prevented mitochondrial dysfunction caused by damage from AAPH. Many other anti-oxidants such as D-methionine, thiourea and coenzyme-Q10 have been studied to prevent SHL induced by oxidative stress 11,12,68. Low or weak mitochondria protection is still the major problem with these anti-oxidant treatments 12. Damaged mitochondria inhibit the synthesis of oxidative phosphorylation complexes, and cells initiate apoptotic cell death, creating further damage to mitochondrial function 69. Therefore, we have shown that the PB-LCA combination could represent one way to counteract mitochondrial dysfunction induced by the free radicals.

Effect on inflammatory profile

The production of inflammatory cytokines TNF-α and IFN-γ are significantly lower in the group treated with F3 micro-nanocapsules, followed by F2. The highest cytokine levels analysed correspond with the

untreated AAPH C2 group ($p > 0.05$) (Fig. 4D-E). Noteworthy is the decrease in TNF-α and IFN-γ were seen in group F3 from 13.76 ± 0.87 pg/mL to 3.26 ± pg/mL and 13.55 ± 0.28 pg/mL to 5.88 ± 0.13 pg/mL respectively, as noted in **Fig. 4D and 4E**. A previous study has reported that inflammation could be one of the most causative factors involved in SHL and is also connected with the growth and progress of the disease 70. In the cochlea, it is well studied that the spiral ligament releases chemokines, including TNF-α and IFN-γ, and their overexpression is seen in oxidative stress, which may cause hair cell function disorder and subsequent SHL 71. IFN-γ causes vestibular hair cell death via different cellular mechanisms, and it may sensitise cochlear cells to TNF-α cytotoxicity 72. Similarly, the same study reported the sensitisation effect of IFN-γ to TNF-α in HEI-OC1 cells and the effect on cochlear sensory cells. Moreover, TNF-α and IFN-γ are key molecules to activate the caspase-dependent apoptotic and their expression is highly present in mitochondrial dysfunction 73. It could be reasonable to assume that cells exposed to AAPH amplify pro-inflammatory cytokines, thus determining diseases severity. The present study successfully decreased the level of pro-inflammatory cytokines when treated with F3 micro-nanocapsule, which is in line with our above cell viability assay (Fig. 3**)** and previous studies 30,48,63.

Effect on cellular oxidation assay

Figure 4F shows the cellular oxidation assay of HEI-OC1 cells over 48 hours for C1, C2, F1, F2 and F3 treatment groups. The cells treated with F3 micro-nanocapsules showed a significant decrease in fluorescent activity, which indicates the combination of PB-LCA brought a significant anti-oxidant activity that inhibited the formation of the intracellular release of peroxyl, hydroxyl or ROS activity that can cause lipid peroxidation induced by AAPH ($p < 0.05$), consistent with our previous findings on pancreatic beta-cell 34,74.

Exposures of HEI-OC1 cells to AAPH significantly affects cell survival and viability, energy production, pro-inflammatory cytokines release and oxidation assay. However, co-treatment of cells with PB micro-nanocapsules protects the cells from damage induced by AAPH. The improved cellular function was noticed more when LCA was added to the PB formulation. This suggests that PB's antioxidant, anti-inflammatory function and cellular uptake are enhanced in the presence of LCA. This in turn results in improvements toHEI-OC1 cell survival, energy production, pro-inflammatory cytokines, and oxidation level.

Conclusion

To our knowledge, this is the first study in which PB-based miro-nanocapsule were developed to examine the effect of PB micro-nanocapsules on oxidative stress in HEI-OC1 cells. This preliminary study showed that the developed method is optimised, robust, and successful in producing uniform micro-nanocapsule without the presence of drug crystals on the capsule surface, with physiochemical compatibility, stability, and controlled and sustained drug release over the time when LCA is added. The addition of LCA does not change the fluid behaviour nor the drug content, but influences the electrokinetic stability, surface chemistry and size of capsules. The *in vitro* study finding showed the addition of LCA on PB micro-nanocapsule significantly improves the biological function of the HEI-OC1 cells, which suggests potential

application in treating SHL induced by oxidative stress. Future studies will be focused on the mechanism of PB on other anti-ROS proteins and enzymes, and *in vivo* studies to show its optimised function in inner hair cells and nervous.

Materials And Methods

Reagents

PB (≥ 99), LCA (≥ 95%), low viscosity sodium alginate (SA; ≥ 99), Tween 80, gelatin, poloxamer, Polyvinyl alcohol (PVA), Poly(acrylic acid) (PAA), polystyrene sulfonate (PSO), *Poly-L-ornithine (PLO)* and silk fibroin protein were gained from Sigma-Aldrich (St Louis, MO, USA). 2,2'-Azobis-2-methyl-propanimidamide, dihydrochloride (AAPH) was bought from Sapphire Bioscience (Redfern, NSW, Australia) and 20,70-Dichlorofluorescin diacetate (DCFH-DA) from Sigma-Aldrich as well. Dulbecco's Eagle's Medium (DMEM) (Bioscience Gibco TM, Dublin, Ireland), foetal bovine serum (Thermofisher Scientific, Melbourne, Australia), MTT(3- (4, 5 - dimethylthiazol-2-yl)-2, 5- diphenyltetrazolium bromide) (Thermo Fisher Scientific MA, USA), (PBS), pH 7.4 (Thermofisher Scientific, Australia), DMSO (Sigma Chemical Co, USA), Hoechst 33258 (Thermofisher Scientific, Australia), propidium iodide (1 µg/ml) dye (Thermofisher Scientific, Australia), seahorse kit (Massachusetts, USA) and cytokine bead array assay (BD Bioscience, CBA Mouse, USA) were brought for cell work.

Preparations of Drug

Stock mixtures for the formulations were prepared in deionised water using PB (0.45% w/v), LCA (0.45% w/v), SA (1.7% w/v), tween 80 (1.7% v/v), gelatin (0.8% w/v), poloxamer (1% w/v), PVA (1.3% w/v), PAA (0.35% w/v), PSS (0.35% v/v), PLO (1.1% v/v) and silk fibroin protein (0.7% w/v). All formulations were mixed thoroughly for 10 hours at room temperature. The stock solutions were stored in the fridge and used within 24 hours of preparation.

Preparation of micro-nanocapsule

Three different formulations were prepared; F1= polymers only, F2= polymers and PB, F3= polymers, PB and LCA. The micro-nanocapsules were prepared by pumping in the formulation at a 5-10% flow rate in the BUCHI mini spray dryer B-290 with a 0.7 mm nozzle diameter (Meierseggstrasse, Flawil, Switzerland). Inlet and outlet temperatures at 150°C to 170°C and 60°C, respectively. The aspirator was set at 92-95%. All the formulations' dry powder was collected, weighed, and used for further analysis. Each experiment was analysed in triplicates (n = 3).

Particle characterization

Toporphology, size and surface elemental analysis of micro-nanocapsules

The size and appearance of micro-nanocapsules were determined using a field emission scanning electron microscope (SEM; CLARA TESCAN, Brno, CZ). The mean particle size was determined by using

the software Image J Analysis. The surface elemental analysis was characterised using energy-dispersive spectrometry (EDS, INCA X-Act; Oxford Instruments, UK). Prior to imaging, dried particles were mounted on an aluminium stub with double-sided adhesive carbon tape and coated under vacuum in an argon atmosphere with 5 nm platinum.

Rheological analysis, zeta-potential, surface tension and physicochemical compatibility

Rheological analyses such as viscosity, torque, shear stress and shear rate were measured for all the formulations using the viscometry (Visco-88 viscometer, Malvern Instruments, Malvern, UK) at various speeds. Particle electrokinetic stability was measured using the Zetasizer 3000 HS (Malvern Instruments, Malvern, UK). Tensiometer (Sigma 703, NSW, Australia) was used to analyse Surface tension.

Powder form compounds and the formulations' physical characterisation were analysed using the differential scanning calorimetry (DSC) (Netzsch DSC 3500 Sirius, JP) under a nitrogen atmosphere. The heat flow difference between reference and sample is determined, representing the sample's caloric change. Briefly, dry samples (F1, F2, F3, individual and mixture of compounds) were sealed in an aluminium pan together with a reference (empty sealed pan) and heated range from 10°C to 300°C at a flow rate of 20 K/minute with auto cooling 35.

The chemical profile of compounds and formulations characterisation was performed by Fourier transform infrared spectroscopy (FT-IR) (Waltham, MA, USA) in a transmission frequency range of 450-4000 cm^{-1} 35.

Drug content and release study

For drug content, 8 mg of F1 and F2 suspensions were stirred at 37°C, 100 rpm for 4 hours in 10 mL acetonitrile. 1 mL of the suspension was filtered and transferred to a glass vial and measured using high-pressure liquid chromatography (HPLC) using the method mentioned below. The amount of drug content and encapsulation efficiency was calculated as described previously 48.

For the PB release study, 100 mg of F2 and F3 micro-nano particles were suspended in 10 mL of perilymph-simulating fluid (pH 7.25 and Osmolarityms= 320 mOsm/L) at 37 °C for 4 hours, stirred at 100 rpm. The fluid was collected in a tube every 30 minutes, and sink conditions were maintained throughout the experiment. The tubes were centrifuged for 30 minutes at 11,000 xg and filtered using a 0.22-µm Millex syringe filter before being injected into HPLC to analyse the release parameters. For HPLC analysis, 20 µL samples were loaded with a low-pressure gradient in the Shimadzu Prominence HPLC system (Pump model: LC-20AT, UV detector: SPD-20A and injector model: SIL-20AC, Shimadzu Corporation, Kyoto, Japan) on a Phenomenex C18 reverse-phase column with an internal diameter of 4.5 mm and a length of 25 cm at a wavelength of 242 nm. The suspension and PB standard concentrations were run in acetonitrile: water (95:5% v/v) at the wavelength of 242nm with a flow rate of 1.5ml/min. PB standard concentrations were run from 0.04 to 12 mg/mL 34.

In vitro study

Cell culture

HEI-OC1 (House Ear Institute-Organ of Corti 1) cells were obtained from UCLA medical centre. Cells were cultured in permissive conditions (33°C and 10% CO_2) in high glucose in DMEM without antibiotics, with 10% foetal bovine serum. At every 24 hours interval, media was changed and when the cells population reached around 80% confluence, a sub-culture was performed as described[75,76].

For each assay, cells were collected and adjusted at 2.0×10^5 cells/mL concentrations and left overnight in incubation for the attachment on the cell-well plate. The experiment started by exposing the cells to a chemical AAPH stressor in various concentrations. The cells' viability was significantly decreased with the increasing concentration of AAPH. AAPH at a 12.5 millimole (mM) rendered a ~50% cell viability (IC_{50}) and this concentration was selected for this study. Cells were then treated with differently prepared micro-nanocapsules (F1, F2 and F3) for 48 hours and compared within the different groups and controls (C1= untreated cells and C2 = cells treated only with AAPH; negative control).

Cell viability assay

Cell viability analysis was performed via MTT assay. The MTT stock solution (5mg/ml) was prepared in PBS. For this assay, cells were collected and adjusted to the required concentration (2.0×10^5 cells/mL). Cells were treated with AAPH and co-treated with micro-nanocapsules. After 48 hours of treatment, MTT assay was performed as mentioned previously with slight modification [76]. Briefly, after 48 hours, cell media was removed, washed with PBS, and 30 µL of MTT reagent was added with serum-free DMEM media and incubated for 3 hours. After 3 hours, DMSO was added to stop the reaction; the multi-well plate was then kept on a plate shaker for another 10-20 minutes to ensure the reaction was completed. PerkinElmer Multimode Plate Readers (Waltham, Massachusetts, USA) set at 550 nm were used to measure the absorbance, and the result was expressed as a normalised percentage of viable cells compared to the control culture cells.

For live/dead cell staining, the cell was seeded on 24 well plates and left overnight to allow attachment to the substrate in an incubator, and then cells were stressed with the addition of AAPH. After 48 hours of the treatment, the cells were washed with PBS, treated with the mixture of Hoechst 33258 (5 µg/ml) and propidium iodide (1 µg/ml) dye, and incubated for another 10 minutes. Fluorescent images were captured by Olympus IX51 inverted fluorescence microscope (Tokyo, JP). For the analysis of sufficient cell numbers to allow the presented data to have statistical significance, images from four adjacent fields were taken per well, and the percentage of the dead and live/cell was calculated. Cells were considered dead if they emitted the fluorescence signal only propidium iodide.

Bioenergetics assay

Mitochondrial function was analysed by measuring oxygen consumption rate (OCR), extracellular acidification rate (ECAR) and proton production rate (PPR) using real-time Seahorse Flux Analyser XF 96 (Seahorse Bioscience, USA) with our well-established method 33. Briefly, the first injection was with media without glucose, with subsequent ATP synthase inhibitor oligomycin (1.5 µM) and FCCP (1 µM) (carbonyl cyanide-p-trifluoromethoxy phenylhydrazone) and the final injection was complex I + II inhibitors Rotenone + antimycin A (0.5 µM) 77. The result was automatically generated and analysed by the wave software.

Cytokine bead array assay

Cytokine release (TNF- α, Tumor necrosis factor-alpha and IFN-γ, interferon-gamma) from 48 hour treated HEI-OC1 cells was performed via the cytokine bead array assay BD Bioscience cytometry bead using the BD FACSCanto II cell analyser 9BD Bioscience, USA) as per protocol provided. Data were analysed by using the FlowJO software (FlowJo, Ashland, OR, USA).

Cellular anti-oxidant assay

This assay measures the anti-oxidant effect on live cells. It is the standard approach to measure intracellular ROS via the use of DCFH-DA. For this assay, after 48 hours of the AAPH treatment and co-treatment with micro-nanocapsules, cells were washed with PBS, treated with 50 µM fluorescence label probe DCFH-DA and incubated for 30 minutes. DCFH-DA stock solution (25 mM) was prepared in methanol, aliquoted and stored at -20°C. DCFH-DA is esterified into DCFH when it diffuses through the cell membrane into the cytosol, which is oxidised by intracellular ROS to form fluorescing DCF. The higher the fluorescence activity, the greater the DCFH-DA oxidation which was measured at 485 nm absorption and 538 nm emission using Enspire Multimode Plate Reader 34,78,79.

Statistical analysis

All the experiments were analysed thrice; data were shown as the mean ± standard deviation (SD) or standard error of deviation (SED) and analysed using one-way analysis of variance (ANOVA) followed by Tukey's posthoc analysis or by using Pearson t-test using Graphpad Prism version 8.1.2. Statistical significance value was set at $p < 0.01$ or $p < 0.05$.

Declarations

Funding

The work is partially supported by the European Union Horizon 2020 research project and innovation program under the Marie Skłodowska-Curie Grant Agreement No 872370. Curtin Faculty ORS-WAHAI Consortium, the Australian National Health and Medical Research (APP9000597).

Acknowledgements

The authors acknowledge the Australian Research Training Program Scholarship for their support. The authors are very grateful to Young Joon Seo, Yonsei University Wonju College of Medicine, South Korea and UCLA medical centre for kindly donating the HEI-OC1 cell line.

Conflicts of interest

Al-Salami H has been and is currently receiving funding from Beijing Nat-Med Biotechnology Co. Ltd. and Glanis PTY Ltd. All other authors have no completing interest to declare.

Availability of data and Materials

The datasets generated and/or analysed during the current study are not publicly available but are available from the corresponding author on reasonable request due to pending commercialization limitation.

Author contributions

Conceptualization, H.A.-S, M.M. and A.M.; Data curation S. R.W, C.M.I, B.K, M.J, P.L, T.F, M.L; Funding acquisition, H.A.-S, M.M. and A.M.; Investigation, all authors; Methodology, S. R.W, C.M.I, B.K, M.J, P.L, T.F and, M.L.; Project administration, H.A.-S, M.M, A.M, E.Y.W and M.D; Resources, H.A.-S, M.M, A.M, E.Y.W and M.D.; Supervision, H.A.-S, M.M, A.M, E.Y.W and M.D.; Validation, S. R.W, CM.I, B.K, M.J, P.L, T.F and, M.L.; Visualization,S. R.W, CM.I, B.K, M.J, P.L, T.F and, M.L.; Writing—original draft, S.RW; Writing—review & editing, all authors. All authors have read and agreed to the published version of the manuscript.

References

1. Henderson, D., Bielefeld, E. C., Harris, K. C. & Hu, B. H. The role of oxidative stress in noise-induced hearing loss. *Ear and hearing* **27**, 1-19, doi:10.1097/01.aud.0000191942.36672.f3 (2006).
2. Menardo, J. *et al.* Oxidative stress, inflammation, and autophagic stress as the key mechanisms of premature age-related hearing loss in SAMP8 mouse Cochlea. *Antioxidants & redox signaling* **16**, 263-274, doi:10.1089/ars.2011.4037 (2012).
3. Elias, T. G. A. *et al.* Evaluation of Oxidative-Stress Pathway and Recovery of Sudden Sensorineural Hearing Loss. *Int Arch Otorhinolaryngol* **25**, e428-e432, doi:10.1055/s-0040-1714130 (2021).
4. Böttger, E. C. & Schacht, J. The mitochondrion: a perpetrator of acquired hearing loss. *Hearing research* **303**, 12-19 (2013).
5. Watanabe, K.-i., Inai, S., Jinnouchi, K., Baba, S. & Yagi, T. Expression of caspase-activated deoxyribonuclease (CAD) and caspase 3 (CPP32) in the cochlea of cisplatin (CDDP)-treated guinea pigs. *Auris Nasus Larynx* **30**, 219-225, doi:https://doi.org/10.1016/S0385-8146(03)00049-X (2003).
6. Alvarado, J. C., Fuentes-Santamaría, V. & Juiz, J. M. Antioxidants and Vasodilators for the Treatment of Noise-Induced Hearing Loss: Are They Really Effective? *Frontiers in cellular neuroscience* **14**, 226-226, doi:10.3389/fncel.2020.00226 (2020).

7. Nakae, S. & Tachibana, M. The cochlea of the spontaneously diabetic mouse. *Archives of oto-rhino-laryngology* **243**, 313-316, doi:10.1007/BF00460208 (1986).
8. Raynor, E. M., Carrasco, V. N., Prazma, J. & Pillsbury, H. C. An assessment of cochlear hair-cell loss in insulin-dependent diabetes mellitus diabetic and noise-exposed rats. *Arch Otolaryngol Head Neck Surg* **121**, 452-456, doi:10.1001/archotol.1995.01890040074012 (1995).
9. Lee, Y. Y. *et al.* Atorvastatin prevents hearing impairment in the presence of hyperlipidemia. *Biochimica et Biophysica Acta (BBA) - Molecular Cell Research* **1867**, 118850, doi:https://doi.org/10.1016/j.bbamcr.2020.118850 (2020).
10. Fukushima, H. *et al.* Cochlear Changes in Patients with Type 1 Diabetes Mellitus. *Otolaryngology–Head and Neck Surgery* **133**, 100-106, doi:10.1016/j.otohns.2005.02.004 (2005).
11. Laurell, G. *et al.* Local administration of antioxidants to the inner ear: Kinetics and distribution11The kinetic study was performed at Institut National de la Santé et de la Recherche Médicale U426, Département de Physiologie, Faculté Xavier Bichat, Université Paris 7, 75018 Paris, France. The autoradiographic study was performed at the Karolinska Hospital, 171 76 Stockholm, Sweden. *Hearing Research* **173**, 198-209, doi:https://doi.org/10.1016/S0378-5955(02)00613-5 (2002).
12. Fujimoto, C. & Yamasoba, T. Mitochondria-Targeted Antioxidants for Treatment of Hearing Loss: A Systematic Review. *Antioxidants* **8**, 109 (2019).
13. Brock, P. R. *et al.* Sodium Thiosulfate for Protection from Cisplatin-Induced Hearing Loss. *N Engl J Med* **378**, 2376-2385, doi:10.1056/NEJMoa1801109 (2018).
14. Tavanai, E. & Mohammadkhani, G. Role of antioxidants in prevention of age-related hearing loss: a review of literature. *European Archives of Oto-Rhino-Laryngology* **274**, 1821-1834 (2017).
15. Kim, S. K. *et al.* The effects of the antioxidant α-tocopherol succinate on cisplatin-induced ototoxicity in HEI-OC1 auditory cells. *International Journal of Pediatric Otorhinolaryngology* **86**, 9-14, doi:https://doi.org/10.1016/j.ijporl.2016.04.008 (2016).
16. Zimetbaum, P., Eder, H. & Frishman, W. Probucol: pharmacology and clinical application. *The Journal of Clinical Pharmacology* **30**, 3-9 (1990).
17. Yamashita, S. & Matsuzawa, Y. Where are we with probucol: a new life for an old drug? *Atherosclerosis* **207**, 16-23 (2009).
18. Heel, R., Brogden, R., Speight, T. & Avery, G. Probucol: A review of its pharmacological properties and therapeutic use in patients with hypercholesterolaemia. *Drugs* **15**, 409-428 (1978).
19. Mamo, J. C. *et al.* Probucol prevents blood-brain barrier dysfunction and cognitive decline in mice maintained on pro-diabetic diet. *Diabetes & vascular disease research* **16**, 87-97, doi:10.1177/1479164118795274 (2019).
20. Wagle, S. R. *et al.* Alginate-based drug oral targeting using bio-micro/nano encapsulation technologies. *Expert Opinion on Drug Delivery*, null-null, doi:10.1080/17425247.2020.1789587 (2020).
21. Yehye, W. A. *et al.* Understanding the chemistry behind the antioxidant activities of butylated hydroxytoluene (BHT): A review. *European journal of medicinal chemistry* **101**, 295-312 (2015).

22. Yang, K.-J. *et al.* Optimized phospholipid-based nanoparticles for inner ear drug delivery and therapy. *Biomaterials* **171**, 133-143, doi:https://doi.org/10.1016/j.biomaterials.2018.04.038 (2018).
23. Maeda, Y., Fukushima, K., Kawasaki, A., Nishizaki, K. & Smith, R. J. Cochlear expression of a dominant-negative GJB2R75W construct delivered through the round window membrane in mice. *Neurosci Res* **58**, 250-254, doi:10.1016/j.neures.2007.03.006 (2007).
24. Zou, J. *et al.* Distribution of lipid nanocapsules in different cochlear cell populations after round window membrane permeation. *Journal of Biomedical Materials Research Part B: Applied Biomaterials* **87B**, 10-18, doi:https://doi.org/10.1002/jbm.b.31058 (2008).
25. Praetorius, M. *et al.* Transsynaptic delivery of nanoparticles to the central auditory nervous system. *Acta oto-laryngologica* **127**, 486-490 (2007).
26. Mittal, R. *et al.* Nanoparticle-based drug delivery in the inner ear: current challenges, limitations and opportunities. *Artificial Cells, Nanomedicine, and Biotechnology* **47**, 1312-1320, doi:10.1080/21691401.2019.1573182 (2019).
27. Mathavan, S., Chen-Tan, N., Arfuso, F. & Al-Salami, H. A comprehensive study of novel microcapsules incorporating gliclazide and a permeation enhancing bile acid: hypoglycemic effect in an animal model of Type-1 diabetes. *Drug delivery* **23**, 2869-2880 (2016).
28. Mikov, M. *et al.* The influence of 3alpha,7alpha-dihydroxy-12-keto-5beta-cholanate on gliclazide pharmacokinetics and glucose levels in a rat model of diabetes. *European journal of drug metabolism and pharmacokinetics* **33**, 137-142, doi:10.1007/BF03191110 (2008).
29. Mooranian, A. *et al.* An advanced microencapsulated system: a platform for optimized oral delivery of antidiabetic drug-bile acid formulations. *Pharmaceutical development and technology* **20**, 702-709 (2015).
30. Stojančević, M., Pavlović, N., Goločorbin-Kon, S. & Mikov, M. Application of bile acids in drug formulation and delivery. *Frontiers in Life Science* **7**, 112-122 (2013).
31. Kovacevic, B. *et al.* The emerging role of bile acids as critical components in nanotechnology and bioengineering: Pharmacology, formulation optimizers and hydrogel-biomaterial applications. *Biomaterials* **283**, 121459, doi:https://doi.org/10.1016/j.biomaterials.2022.121459 (2022).
32. Mooranian, A. *et al.* The biological effects of the hypolipidaemic drug probucol microcapsules fed daily for 4 weeks, to an insulin-resistant mouse model: potential hypoglycaemic and anti-inflammatory effects. *Drug delivery and translational research* **8**, 543-551 (2018).
33. Mooranian, A. *et al.* Advanced bile acid-based multi-compartmental microencapsulated pancreatic β-cells integrating a polyelectrolyte-bile acid formulation, for diabetes treatment. *Artificial cells, nanomedicine, and biotechnology* **44**, 588-595 (2016).
34. Wagle, S. R. *et al.* Pharmacological and Biological Study of Microencapsulated Probucol-Secondary Bile Acid in a Diseased Mouse Model. *Pharmaceutics* **13**, 1223 (2021).
35. Wagle, S. R. *et al.* Micro-Nano formulation of bile-gut delivery: rheological, stability and cell survival, basal and maximum respiration studies. *Scientific Reports* **10**, 7715, doi:10.1038/s41598-020-64355-z (2020).

36. Piu, F. & Bishop, K. M. Local drug delivery for the treatment of neurotology disorders. *Frontiers in cellular neuroscience* **13**, 238 (2019).
37. Malamatari, M., Charisi, A., Malamataris, S., Kachrimanis, K. & Nikolakakis, I. Spray Drying for the Preparation of Nanoparticle-Based Drug Formulations as Dry Powders for Inhalation. *Processes* **8**, 788 (2020).
38. Malamatari, M., Somavarapu, S., Kachrimanis, K., Buckton, G. & Taylor, K. M. G. Preparation of respirable nanoparticle agglomerates of the low melting and ductile drug ibuprofen: Impact of formulation parameters. *Powder Technology* **308**, 123-134, doi:https://doi.org/10.1016/j.powtec.2016.12.007 (2017).
39. Mooranian, A., Negrulj, R., Arfuso, F. & Al-Salami, H. The effect of a tertiary bile acid, taurocholic acid, on the morphology and physical characteristics of microencapsulated probucol: potential applications in diabetes: a characterization study. *Drug delivery and translational research* **5**, 511-522 (2015).
40. Mooranian, A. *et al.* Microencapsulation as a novel delivery method for the potential antidiabetic drug, Probucol. *Drug design, development and therapy* **8**, 1221 (2014).
41. Draget, K. I. & Taylor, C. Chemical, physical and biological properties of alginates and their biomedical implications. *Food Hydrocolloids* **25**, 251-256 (2011).
42. Pamies, R., Schmidt, R. R., Martínez, M. d. C. L. & de la Torre, J. G. The influence of mono and divalent cations on dilute and non-dilute aqueous solutions of sodium alginates. *Carbohydrate Polymers* **80**, 248-253 (2010).
43. Mooranian, A. *et al.* An optimized probucol microencapsulated formulation integrating a secondary bile acid (deoxycholic acid) as a permeation enhancer. *Drug design, development and therapy* **8**, 1673 (2014).
44. Mooranian, A. *et al.* Stability and Release Kinetics of an Advanced Gliclazide-Cholic Acid Formulation: The Use of Artificial-Cell Microencapsulation in Slow Release Targeted Oral Delivery of Antidiabetics. *J Pharm Innov* **9**, 150-157, doi:10.1007/s12247-014-9182-5 (2014).
45. Honary, S. & Zahir, F. Effect of zeta potential on the properties of nano-drug delivery systems-a review (Part 2). *Tropical Journal of Pharmaceutical Research* **12**, 265-273 (2013).
46. Xie, H. G. *et al.* Effect of surface wettability and charge on protein adsorption onto implantable alginate-chitosan-alginate microcapsule surfaces. *J Biomed Mater Res A* **92**, 1357-1365, doi:10.1002/jbm.a.32437 (2010).
47. Azarbayjani, A. F., Jouyban, A. & Chan, S. Y. Impact of surface tension in pharmaceutical sciences. *Journal of pharmacy & pharmaceutical sciences* **12**, 218-228 (2009).
48. Wagle, S. R. *et al.* Pharmacological and Advanced Cell Respiration Effects, Enhanced by Toxic Human-Bile Nano-Pharmaceuticals of Probucol Cell-Targeting Formulations. *Pharmaceutics* **12**, 708 (2020).
49. Ajun, W., Yan, S., Li, G. & Huili, L. Preparation of aspirin and probucol in combination loaded chitosan nanoparticles and in vitro release study. *Carbohydrate Polymers* **75**, 566-574 (2009).

50. Bergo, P. & Sobral, P. Effects of plasticizer on physical properties of pigskin gelatin films. *Food Hydrocolloids* **21**, 1285-1289 (2007).
51. da Almeida, P. F., da Silva Lannes, S. C., Calarge, F. A., da Brito Farias, T. M. & Santana, J. C. C. FTIR characterization of gelatin from chicken feet. *Journal of chemistry and chemical engineering* **6**, 1029 (2012).
52. Sockalingam, K. & Abdullah, H. in *AIP Conference Proceedings.* 020053 (AIP Publishing LLC).
53. Alhosseini, S. N. *et al.* Synthesis and characterization of electrospun polyvinyl alcohol nanofibrous scaffolds modified by blending with chitosan for neural tissue engineering. *Int J Nanomed* **7**, 25 (2012).
54. Es-haghi, H., Bouhendi, H., Bagheri-Marandi, G., Zohurian-Mehr, M. J. & Kabiry, K. Cross-Linked Poly(acrylic acid) Microgels from Precipitation Polymerization. *Polymer-Plastics Technology and Engineering* **49**, 1257-1264, doi:10.1080/03602559.2010.496421 (2010).
55. Mooranian, A. *et al.* Single-Cellular Biological Effects of Cholesterol-Catabolic Bile Acid-Based Nano/Micro Capsules as Anti-Inflammatory Cell Protective Systems. *Biomolecules* **12**, doi:10.3390/biom12010073 (2022).
56. Laity, P., Gilks, S. & Holland, C. Rheological behaviour of native silk feedstocks. *Polymer* **67**, 28-39 (2015).
57. Mooranian, A. *et al.* The Effects of Accelerated Temperature-Controlled Stability Systems on the Release Profile of Primary Bile Acid-Based Delivery Microcapsules. *Pharmaceutics* **13**, doi:10.3390/pharmaceutics13101667 (2021).
58. Huang, X. & Brazel, C. S. On the importance and mechanisms of burst release in matrix-controlled drug delivery systems. *Journal of Controlled Release* **73**, 121-136, doi:https://doi.org/10.1016/S0168-3659(01)00248-6 (2001).
59. Shively, M. L., Coonts, B. A., Renner, W. D., Southard, J. L. & Bennett, A. T. Physico-chemical characterization of a polymeric injectable implant delivery system. *Journal of Controlled Release* **33**, 237-243, doi:https://doi.org/10.1016/0168-3659(94)00097-E (1995).
60. Jeong, B., Bae, Y. H. & Kim, S. W. Drug release from biodegradable injectable thermosensitive hydrogel of PEG–PLGA–PEG triblock copolymers. *Journal of controlled release* **63**, 155-163 (2000).
61. Pyykkö, I., Zou, J., Schrott-Fischer, A., Glueckert, R. & Kinnunen, P. An overview of nanoparticle based delivery for treatment of inner ear disorders. *Auditory and Vestibular Research*, 363-415 (2016).
62. Szeto, B. *et al.* Inner ear delivery: Challenges and opportunities. *Laryngoscope Investig Otolaryngol* **5**, 122-131, doi:10.1002/lio2.336 (2019).
63. Mooranian, A. *et al.* Bile acid bio-nanoencapsulation improved drug targeted-delivery and pharmacological effects via cellular flux: 6-months diabetes preclinical study. *Scientific Reports* **10**, 106, doi:10.1038/s41598-019-53999-1 (2020).
64. Yao, B. *et al.* The protective effect of lithocholic acid on the intestinal epithelial barrier is mediated by the vitamin D receptor via a SIRT1/Nrf2 and NF-κB dependent mechanism in Caco-2 cells. *Toxicology Letters* **316**, 109-118, doi:https://doi.org/10.1016/j.toxlet.2019.08.024 (2019).

65. Ward, J. B. J. *et al.* Ursodeoxycholic acid and lithocholic acid exert anti-inflammatory actions in the colon. *Am J Physiol-Gastr L* **312**, G550-G558, doi:10.1152/ajpgi.00256.2016 (2017).
66. Moreira Gomes, M. D. *et al.* 2, 2'-azobis (2-amidinopropane) dihydrochloride is a useful tool to impair lung function in rats. *Frontiers in Physiology* **7**, 475 (2016).
67. Brand, M. D. & Nicholls, D. G. Assessing mitochondrial dysfunction in cells. *Biochemical Journal* **435**, 297-312 (2011).
68. Joachims, H. Z., Segal, J., Golz, A., Netzer, A. & Goldenberg, D. Antioxidants in treatment of idiopathic sudden hearing loss. *Otology & neurotology* **24**, 572-575 (2003).
69. Lyu, A.-R. *et al.* Hearing Impairment in a Mouse Model of Diabetes Is Associated with Mitochondrial Dysfunction, Synaptopathy, and Activation of the Intrinsic Apoptosis Pathway. *International Journal of Molecular Sciences* **22**, 8807 (2021).
70. Fujioka, M. *et al.* Proinflammatory cytokines expression in noise-induced damaged cochlea. *J Neurosci Res* **83**, 575-583, doi:10.1002/jnr.20764 (2006).
71. Sziklai, I., Batta, T. J. & Karosi, T. Otosclerosis: an organ-specific inflammatory disease with sensorineural hearing loss. *European Archives of Oto-Rhino-Laryngology* **266**, 1711-1718, doi:10.1007/s00405-009-0967-y (2009).
72. Moon, S. K., Woo, J. I. & Lim, D. J. Involvement of TNF-α and IFN-γ in Inflammation-Mediated Cochlear Injury. *Ann Otol Rhinol Laryngol* **128**, 8s-15s, doi:10.1177/0003489419837689 (2019).
73. Yang, X. *et al.* Induction of caspase 8 by interferon γ renders some neuroblastoma (NB) cells sensitive to tumor necrosis factor-related apoptosis-inducing ligand (TRAIL) but reveals that a lack of membrane TR1/TR2 also contributes to TRAIL resistance in NB. *Cancer research* **63**, 1122-1129 (2003).
74. Mooranian, A. *et al.* Novel nano-encapsulation of probucol in microgels: scanning electron micrograph characterizations, buoyancy profiling, and antioxidant assay analyses. *Artif Cells Nanomed Biotechnol* **46**, S741-s747, doi:10.1080/21691401.2018.1511571 (2018).
75. Kalinec, G., Thein, P., Park, C. & Kalinec, F. HEI-OC1 cells as a model for investigating drug cytotoxicity. *Hearing Research* **335**, 105-117, doi:https://doi.org/10.1016/j.heares.2016.02.019 (2016).
76. Kalinec, G. M., Park, C., Thein, P. & Kalinec, F. Working with Auditory HEI-OC1 Cells. *J Vis Exp*, doi:10.3791/54425 (2016).
77. Wu, M. *et al.* Multiparameter metabolic analysis reveals a close link between attenuated mitochondrial bioenergetic function and enhanced glycolysis dependency in human tumor cells. *American Journal of Physiology-Cell Physiology* **292**, C125-C136 (2007).
78. Wolfe, K. L. & Liu, R. H. Cellular antioxidant activity (CAA) assay for assessing antioxidants, foods, and dietary supplements. *J Agric Food Chem* **55**, 8896-8907, doi:10.1021/jf0715166 (2007).
79. Yarnpakdee, S., Benjakul, S., Kristinsson, H. G. & Bakken, H. E. Preventive effect of Nile tilapia hydrolysate against oxidative damage of HepG2 cells and DNA mediated by H2O2 and AAPH. *Journal of Food Science and Technology* **52**, 6194-6205 (2015).

Figures

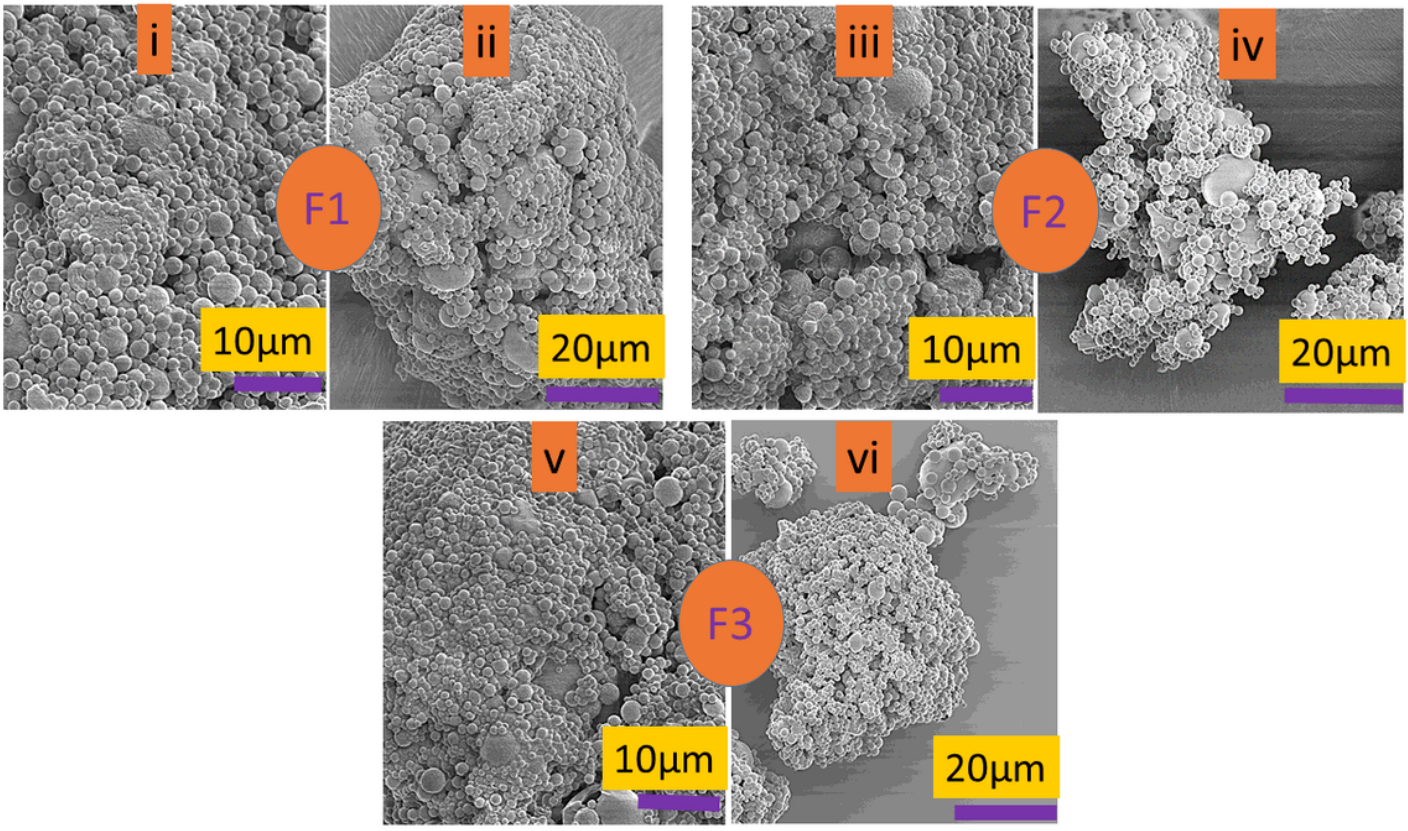

Figure 1

Surface morphology of micro-nanocapsule by SEM of different formulations F1, F2 and F3 (i-vi) at different magnifications, (i, iii and V) 10 µm scale and (ii, iv and vi) 20 µm scale.

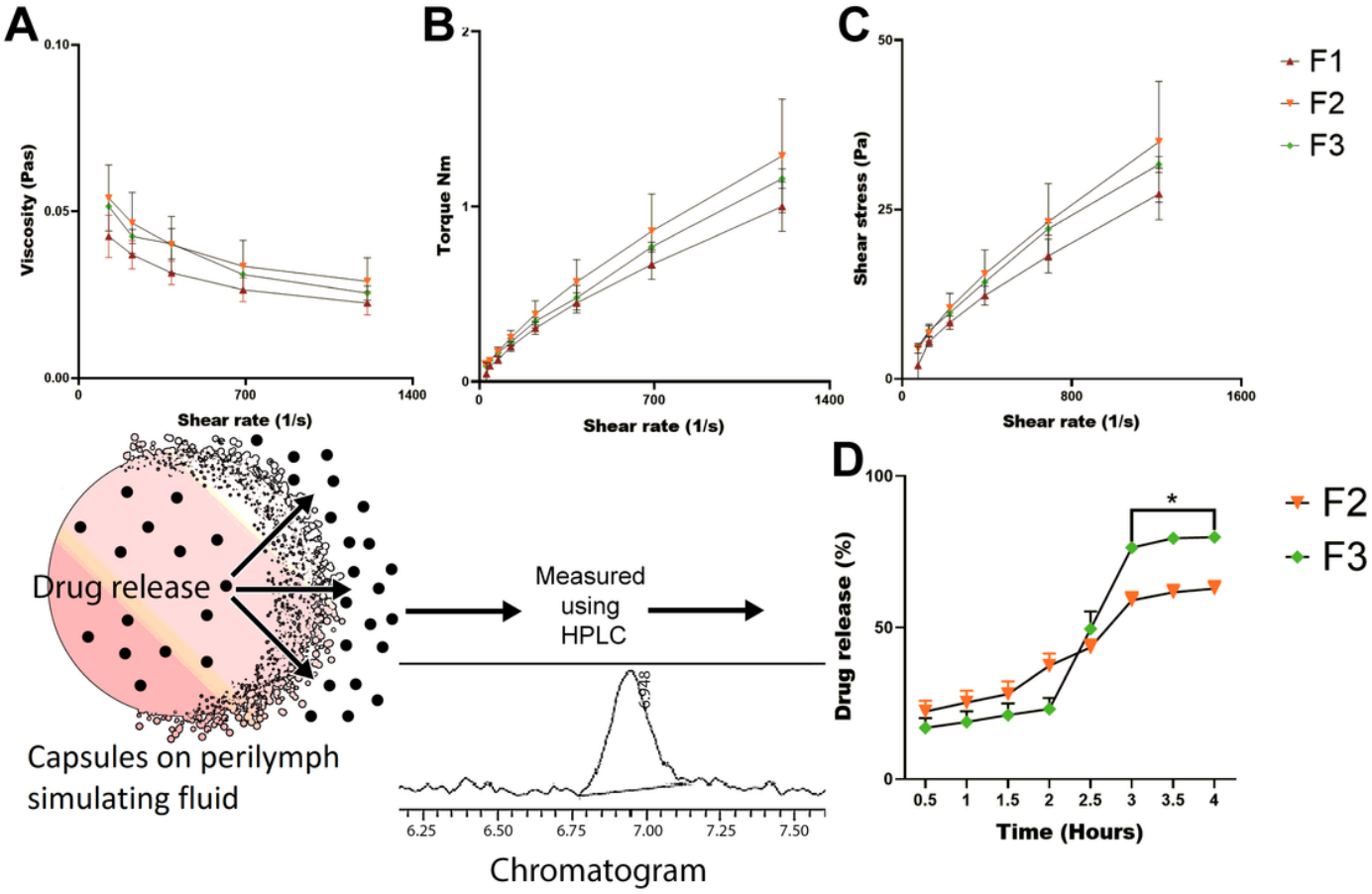

Figure 2

Rheological analysis of different formulations taken at various speeds (A-C) and drug release profile in perilymph-simulating fluid at 37 °C for 4 hours (D). Data are presented as mean ± standard deviation, n = 3. Level of significance, $p < 0.05$

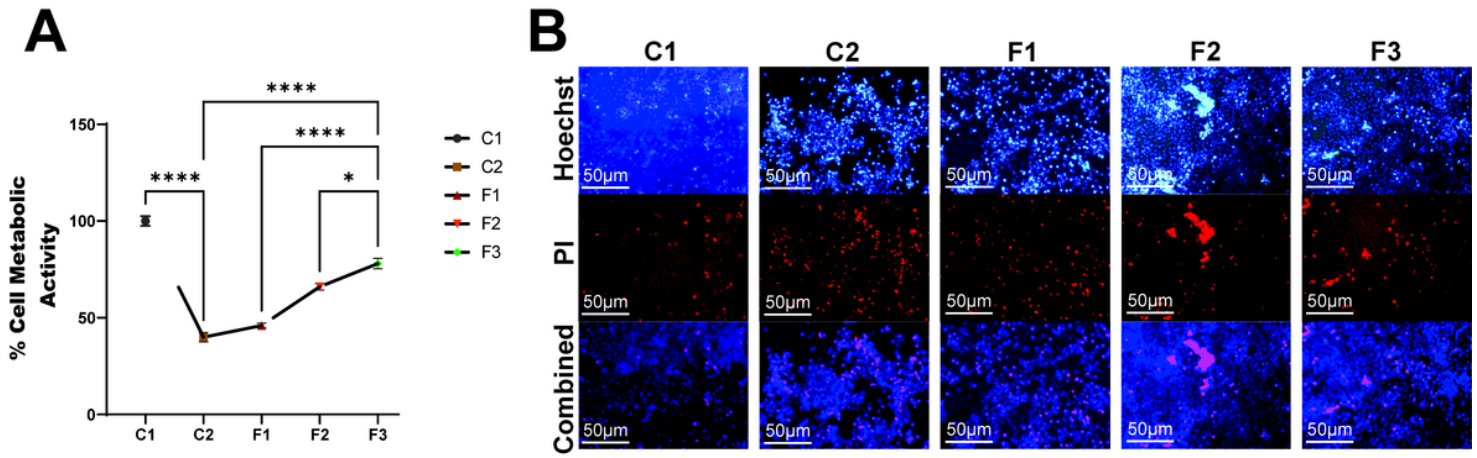

Figure 3

HEI-OC1 auditory cellular viability assay (A) measured by MTT after 48 hours of the treatment and live, death cells imaging confirmed by cell staining assay; blue (Hoechst 33258) and red (propidium iodide) (B). Data are presented as mean ± standard error of deviation, n = 3 Number of * signifies the level of significance ($p < 0.05$ or $p < 0.01$).

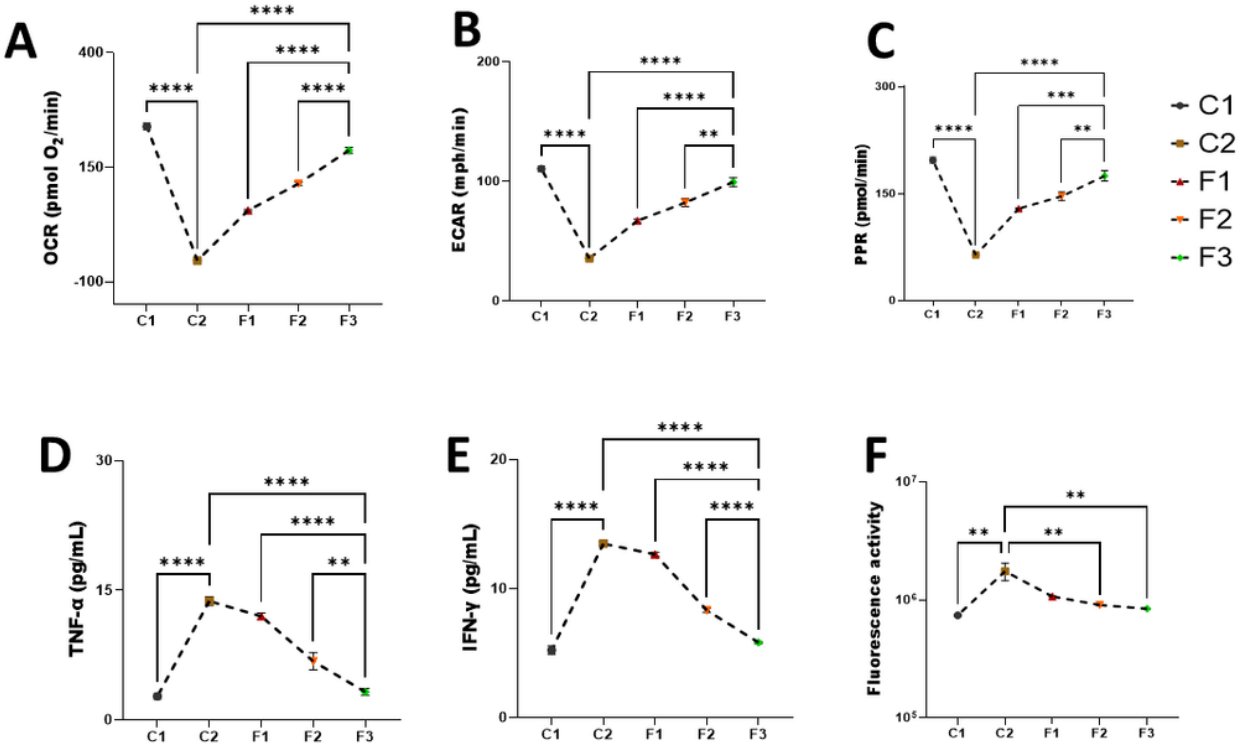

Figure 4

HEI-OC1 auditory cell, bioenergetics assay (A-C), pro-inflammatory assay (D-E) and cellular oxidation assay (F) after 48 hours of cell treatment. Data are presented as mean ± standard error of deviation, n = 3. Number of * signifies the level of significance ($p < 0.05$ or $p < 0.01$).

Supplementary Files

This is a list of supplementary files associated with this preprint. Click to download.

- GraphicalAbstract.jpg